Spectral Anomaly Methods for Aerial Detection using KUT Nuisance Rejection

R. S. Detwiler, D. M. Pfund, M. J. Myjak, J. A. Kulisek, C. E. Seifert

Pacific Northwest National Laboratory, Richland, Washington, 99352, United States

Abstract

This work discusses the application and optimization of a spectral anomaly method for the real-time detection of gamma radiation sources from an aerial helicopter platform. Aerial detection presents several key challenges over ground-based detection. For one, larger and more rapid background fluctuations are typical due to higher speeds, larger field of view, and geographically induced background changes. As well, the possible large altitude or stand-off distance variations cause significant steps in background count rate as well as spectral changes due to increased gamma-ray scatter with detection at higher altitudes. The work here details the adaptation and optimization of the PNNL-developed algorithm NSCRAD (Nuisance-Rejecting Spectral Comparison Ratios for Anomaly Detection), a spectral anomaly method previously developed for ground-based applications, for an aerial platform. The algorithm has been optimized for two multi-detector systems; a NaI(Tl)-detector based system and a CsI detector array. The optimization here details the adaptation of the spectral windows for a particular set of target sources to aerial detection and the tailoring for the specific detectors. As well, the methodology and results for background rejection methods optimized for the aerial gamma-ray detection using Potassium, Uranium and Thorium (KUT) nuisance rejection is shown. Results indicate that use of a realistic KUT nuisance rejection may eliminate metric rises due to background magnitude

and spectral steps encountered in aerial detection due to altitude changes and geographically induced steps such as at land-water interfaces.

Keywords: Spectral Anomaly Detection, KUT Nuisance Rejection, Aerial Search, Aerial Detection, Radiation Detection

1.0 Introduction

Aerial detection combines all the challenges of standoff detection with all the difficulties of mobile survey, including large and varying standoff distances and abrupt and significant changes in background. Critical issues for aerial detection include land-water interfaces, rapidly changing KUT backgrounds, and varying down scatter with altitude changes. To address these issues a spectral anomaly method has been adapted to aerial detection. The NSCRAD (Nuisance-Rejection Spectral Comparison Ratio) algorithm was initially developed at PNNL for medium resolution detectors [1]. The algorithm has been used for a range of ground-based detection applications, including ground-based detection, portal monitoring, and OSI applications [2,3,4,5]. The method used in NSCRAD includes both optimized energy windows for detection of threat sources and a nuisance rejection capability. The spectral anomaly method was optimized in this work for aerial detection systems to increase the probability of detection of threat sources in aerial search while using the nuisance rejection capability to minimize false alarms from rapidly changing aerial background. The implementation of NSCRAD for aerial detection requires optimizing energy windows, adapting KUT nuisance rejection for aerial backgrounds, developing new methods for background tracking, and adjusting tracking and detection thresholds.

2.0 Methodology

2.1 NSCRAD Method

Previous methods have been developed for detection of anomalies in spectra [6]. The specific methodology used here by NSCRAD involves the following steps [1,7]. First, spectral windows are optimized for a given set of threat and nuisance sources by maximizing the differences between these categories as measured by the windows [7]. The process involves both optimization of detection of the threat sources and rejection of the background and nuisance sources [8]. Nuisance sources typically include background components ^{40}K, ^{238}U and ^{232}Th (KUT) and progeny, but may also include medical or industrial sources. An example set of windows is shown in Figure 1.

Next, the vector of background-scaled spectral comparison ratios (SCRs) is calculated for each spectra or sample time. The SCR's are count rate differences between spectral windows, scaled by the mean backgrounds, as shown here:

(1) $$c_{\alpha(1,2)} = c_1 - \frac{\mu_1}{\mu_2} c_2,$$

where μ is the mean background and the numerals in the subscripts refer to the different spectral windows. Next, vector SCRs are calculated for the Naturally Occuring Radioactive Material (NORM) and assumed nuisance spectra, and these components are removed from the sample spectra using an orthogonal subspace projection:

(2) $$\mathbf{P}_\alpha = \mathbf{A}_\alpha (\mathbf{A}_\alpha^T \boldsymbol{\Sigma}_\alpha^{-1} \mathbf{A}_\alpha)^{-1} \mathbf{A}_\alpha^T \boldsymbol{\Sigma}_\alpha^{-1}, \quad \mathbf{A}_\alpha = \begin{bmatrix} \mathbf{a}_{\alpha 1} & \mathbf{a}_{\alpha 2} & \mathbf{a}_{\alpha 3} & \mathbf{a}_{\alpha 4} \end{bmatrix}.$$

Here, ∑ is the background covariance. Finally, the standardized distance metric is calculated, and weighted by background covariance as shown below; an observed value above a given threshold, D, indicates threat or anomalous source.

(3)

$$D = \sqrt{\mathbf{c}_\alpha^T \boldsymbol{\Sigma}_\alpha^{-1} (\mathbf{c}_\alpha - \mathbf{P}_\alpha \mathbf{c}_\alpha)}$$

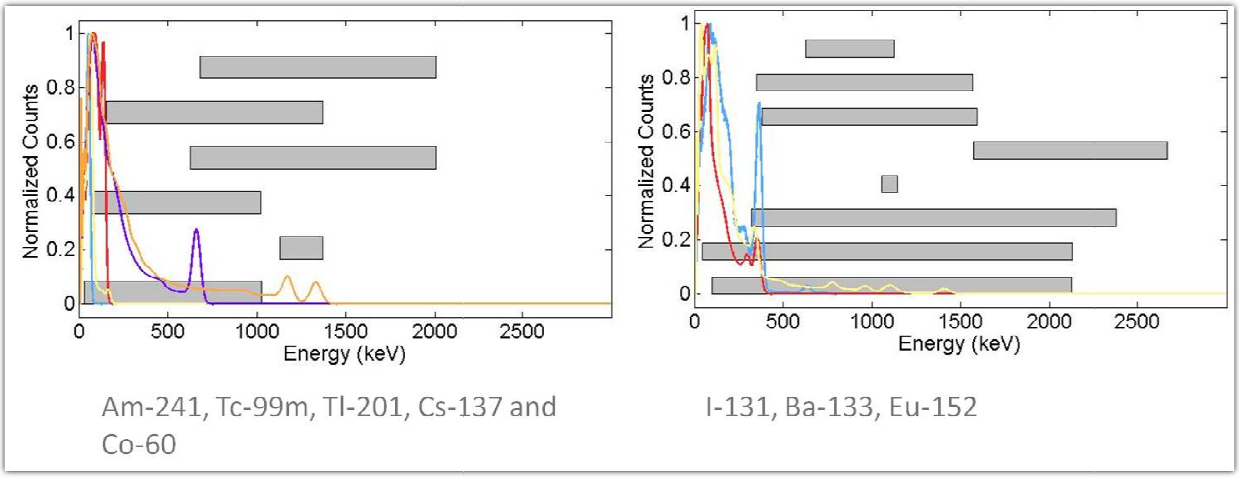

Figure 1. Example of NSCRAD Energy windows for two sets of threat sources, with KUT rejection.

2.2 General Approach

The spectral anomaly method NSCRAD was optimized for two helicopter-based gamma-ray detection systems using NaI(Tl) and CsI(Na) detector arrays. The adaptation of the spectral anomaly method NSCRAD for aerial detector systems involves both optimization of the background rejection methodology for aerial detection as well as optimization of parameters related to source detection. An important factor in source detection, which varies with stand-off distance and speed, is the integration time used in the algorithm; this time was optimized through analysis using source injections to a value of 3 seconds. This factor agreed with past calculations based on speed and offset [9]. The background rejection methodology and settings were investigated using aerial background flyover data from a NaI(Tl) based detector system spanning a large altitude range of 30 m to 400 m and involving two flight locations. We examined whether the NSCRAD settings need to be adjusted with altitude and location. The spectral

ROI's for a set of target sources were also optimized for the particular detection system using simulated spectra at a typical flight altitude of 300 ft.

The results with re-optimization of windows and addition of background K, U and Th nuisance rejection based on the particular detector system showed a significant reduction in the background-induced jumps in the NSCRAD metric corresponding to altitude changes. The results also indicated that with realistic nuisance rejection and energy windows optimization, no altitude dependent thresholds were needed.

2.3 Background Tracking and Detection Threshold Optimization

Two established methods for background tracking with NSCRAD were adapted for the aerial detection applications described here [9]. One is the Rolling Sum using a 60 second time constant, based on the following equation:

$$\hat{\mathbf{B}}_k = \frac{1}{60}\sum_{j=0}^{59}\mathbf{B}_{k-j} \quad (4)$$

The second is the Exponentially Weighted Moving Average (EWMA):

$$\hat{\mathbf{B}}_k = (1-\lambda)\hat{\mathbf{B}}_{k-1} + \lambda\mathbf{B}_k \quad (5)$$

The exponential constant here is set to a value of 0.0443 to match the 50% power cutoff frequency of the EWMA to that of a 60s rolling average. The value of 60 seconds was chosen from optimization studies using source injections on real flight background data for the NaI(Tl) – based detector system.

Detection and tracking thresholds were set using available flight data for the detector system, and balancing the percent of false positives [9]. The data included two sets of flight data, in two different geographic locations, spanning altitude ranges of 50 ft above ground level (AGL) to

600-700 ft AGL, with a combined total of over 10,000 data points. Below in Figure 2 is an illustration of the method for one geographic location, of 9,300 data points. The method illustrates the requirements of setting the alarm and tracking thresholds based the allowed number of false positives. The metrics are shown for three sets of energy windows, corresponding to specific low, medium and high energy sources.

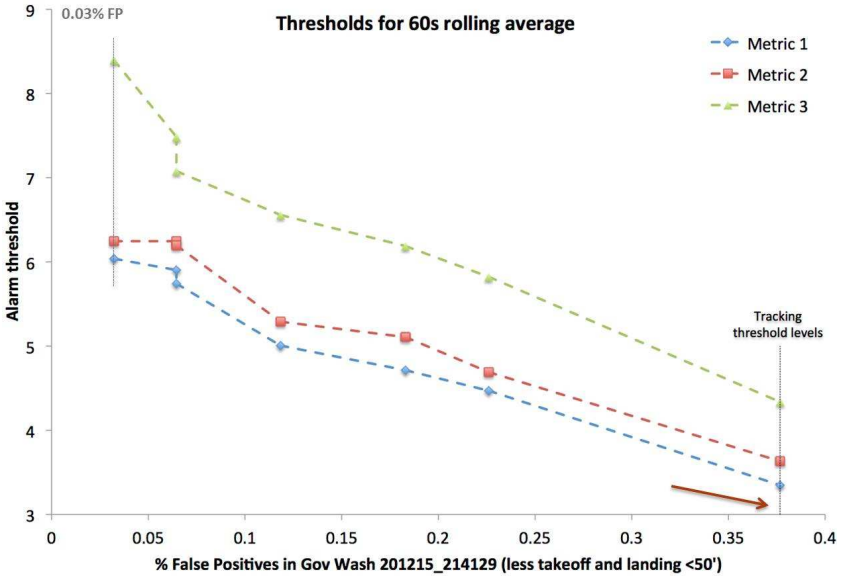

Figure 2. Balancing alarm thresholds vs. false positive rates for the rolling 60 second background method.

3.0 Results

3.1 Window Optimization

A comparison of the NSCRAD metric before and after the adapted KUT background rejection and window optimization for a particular set of energy for detection of ^{133}Ba and ^{131}I is shown in Figure 3. Here, results on the left use generic energy windows for large NaI(Tl) detector geometries from land-based applications. Results on the right use energy windows which are

optimized for a similar detector geometry, but for aerial applications. The new windows were developed using the adjusted detector response function based on air attenuation and scatter, using real flight data from the NaI(Tl)-based aerial detector system at a range of flying altitudes.

NSCRAD metric results from real flight data from this system are shown below, using previous generic land-based windows on the left and windows optimized for the aerial detector system on the right. This data set included several real medical/industrial sources as indicated by the elevated metrics in the figure; these are detected by both sets of parameters. However, other metric rises shown in the left figure are associated with altitude or background changes; these are reduced or eliminated with the addition of the KUT nuisance rejection and re-optimized energy windows. In addition, an important result from adaptation of windows for aerial detector response function is that since the metric rises from background and altitude changes are minimized with aerial energy windows, altitude-dependent thresholds are not required.

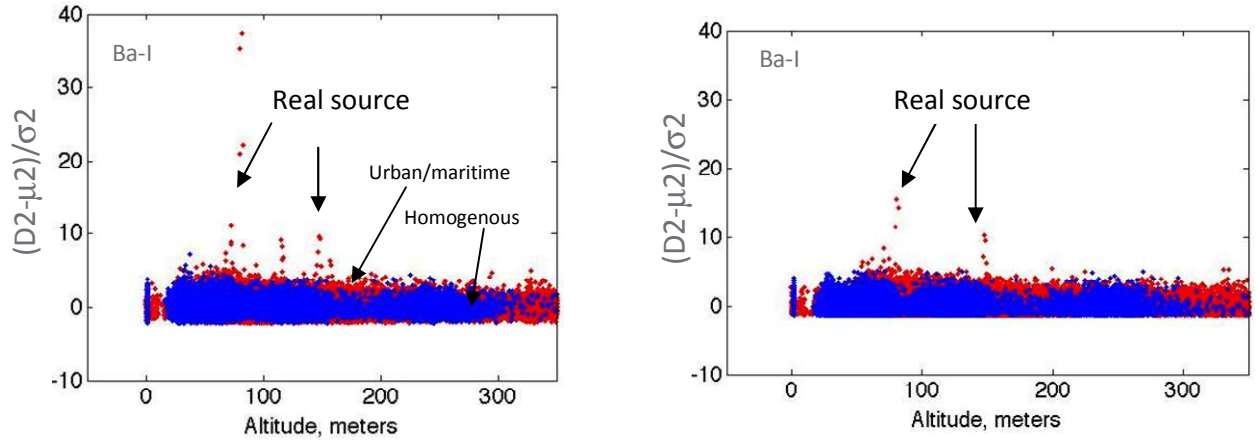

Figure 3. Comparison of NSCRAD Metrics without optimization (left) and with optimization for aerial applications (right), as a function of altitude for data from an urban/maritime area and a relatively homogeneous background area.

An example showing the importance of adapting spectral anomaly windows for the detector system geometry specifications is shown below. Here, analysis is shown for simulated flight data using simulated background, with source injections, as has been done with past NSCRAD sensitivity comparisons [9,10]. Source injections included Cs-137 and Co-60 source of varying strengths. Results in Figure 4 show a comparison of the analysis with two sets of windows, both optimized for aerial detection at similar altitude ranges, but for different detector geometries. Windows on the left are based on a NaI(Tl) array of large crystals, while windows on the right are based on a CsI array with smaller detector geometries.

The simulated background was developed using measured ratios of KUT components from flight data form the NaI(Tl) based detector system over a relatively homogenous background. The background spectral response was simulated for a new detector geometry, based on an array of CsI detectors of smaller detector geometries, using the measured KUT concentrations. Next, simulated second-by-second flight data was developed using simulated background spectra with Poisson variation added, and injections of source spectra were made using simulated detector responses for a particular flight altitude and source offset. Figure 4 shows a comparison of the analysis with two sets of windows, at a flight altitude of 300 ft AGL, for both zero and 300 ft offsets. There is an approximately 30% gain in sensitivity, taken as the ratio of the source metric to the average background, using the energy windows adapted to new detector geometry.

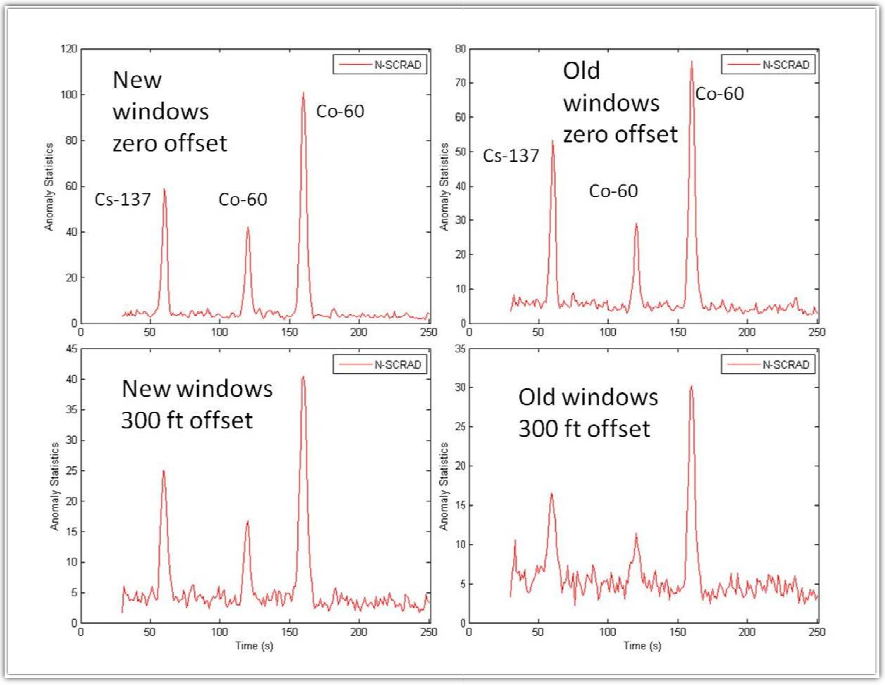

Figure 4. Comparison of NSCRAD metric results using aerial windows optimized for a CsI-based detector geometry (left) and aerial NaI(Tl)-based windows (right) using simulated flight data for the CsI-based detector system.

3.2 KUT Background Rejection Optimization

3.2.1 Analysis of Performance with Artificial Background Steps

As part of the optimization for aerial detection, analysis involving real and induced background magnitude and spectral steps, such as those encountered at a land-water interface, was conducted. Initial analysis involved artificially induced background steps of both count rate and of an individual background spectral component. This analysis allowed a controlled evaluation of performance of the NSCRAD background rejection capabilities. Here, background flight data was generated for the 12 detector NaI(Tl) system using simulated background spectra from measured KUT concentrations at 100 ft AGL for an area of relatively homogeneous background,

with Poisson variation added. NSCRAD analysis was conducted using the two background methods. For both methods, background tracking thresholds were set for the NaI(Tl)-based detector system using real flight data. Metric results from a 5 X background step in count rate only is shown in Figure 5; here the relative background spectral components are kept constant (with addition of Poisson variation). The results without nuisance rejection are labeled as SCRAD; results with nuisance rejection are labeled as NSCRAD. A correction to the covariance matrix based on the gross count rate was also applied for these results [9]. Metric results are scaled by a detection threshold set for the NaI(Tl) system from real flight data, with a value of one corresponding to a detection. The results show some sensitivity to the background step without nuisance rejection, with some difference in this example between the two background methods. However, for both methods, NSCRAD results (with nuisance rejection) reduce the metric at the spectral step to a value at or below the detection threshold.

Metric results from a 5 X step in an individual spectral component are shown in Figures 6 and 7; here a single spectral component is varied, while keeping the background count rate constant. Results from steps in K-40 have a close similarity in the SCRAD results (without nuisance rejection) between background methods (Figure 6). Steps in ^{238}U and ^{232}Th (Figure 7) show some differences in the SCRAD responses between background methods. However, in all cases the SCRAD response show sensitivity to the background step, with a metric above the detection threshold, as the step differs spectrally from the background. In all cases the NSCRAD metric (with KUT nuisance rejection) shows a similar response for both methods, and a significant reduction in the metric at the step, reducing the metric to below the detection threshold.

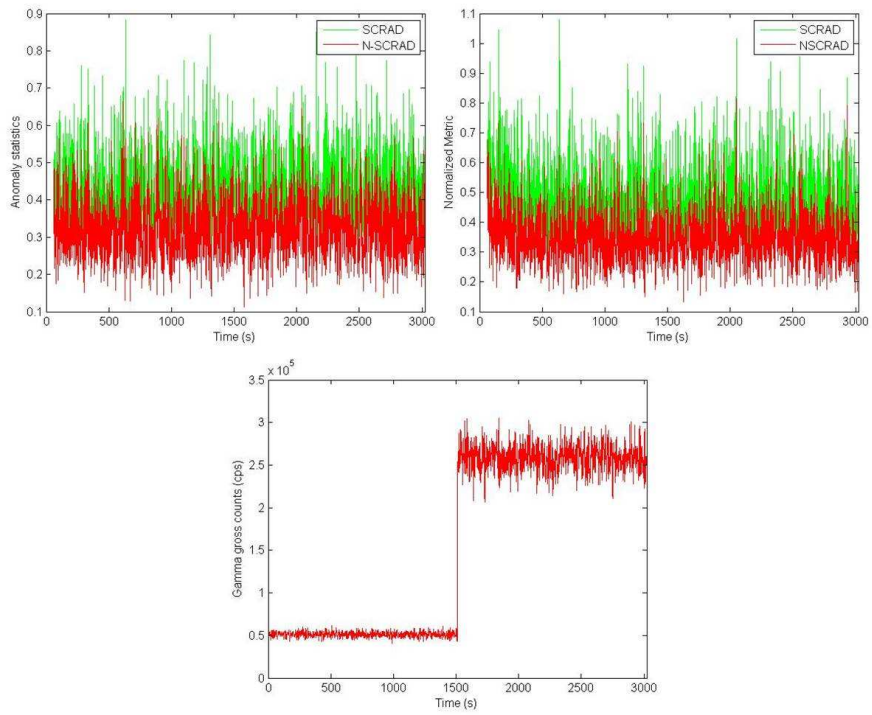

Figure 5. Results with and without nuisance rejection for an artificially induced 5X count rate step.

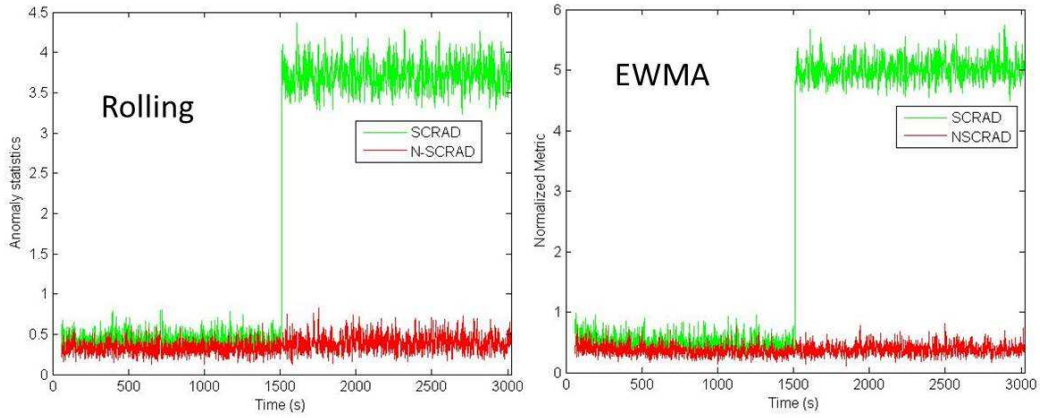

Figure 6. Results with and without nuisance rejection for an artificially induced 5X spectral step in K-40.

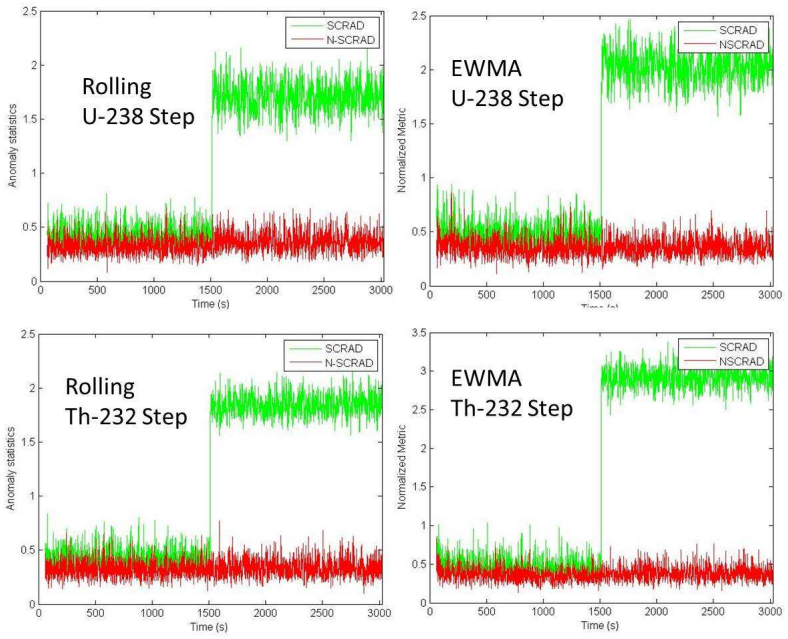

Figure 7. Results with / without nuisance rejection for 5X spectral step in ^{238}U-and ^{232}Th.

3.2.2 Background Tracking Thresholds

As described in section 2.2, the above analysis used a background tracking threshold that was optimized for the NaI(Tl)-based detector system. Figure 8 illustrates the effect on varying tracking thresholds on the SCRAD and NSCRAD metrics. The responses for the EWMA background tracking method are shown for a 5 X step in the ^{238}U background component, for three sets of thresholds. Results are shown for the optimized threshold, one-half and 2X the threshold. It is apparent that lower tracking thresholds increase the SCRAD response to the induced background step, while higher thresholds reduce the response to the step. However, higher thresholds may also reduce the NSCRAD responses to real sources. As seen, for low, optimum and high tracking thresholds, the NSCRAD response (with nuisance rejection) does significantly reduce the metric value at the background step.

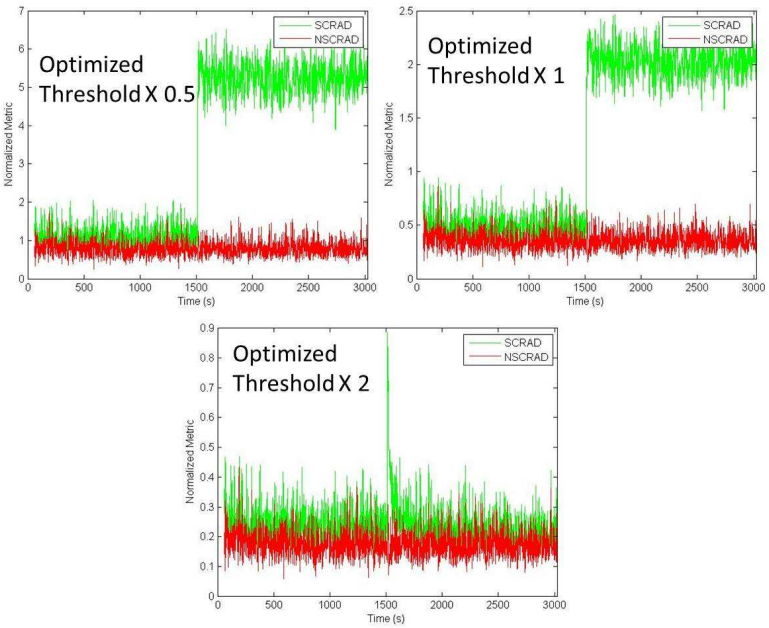

Figure 8. Effects of Background tracking Threshold on SCRAD/NSCRAD Response for 5X Step in ^{238}U.

3.2.3 KUT Rejection with Land/Water Interface

An example of the background rejection response of the algorithm to real flight data over a land/water interface using optimized KUT nuisance rejection is shown in Figure 9. The flight data, with gross count rates shown at the left, is from a 12-detector NaI(Tl) array, and contained multiple count rate jumps due to repeated passes over the land-water interface. The NSCRAD metric response is shown on the right, using the two background methods mentioned above, with EWMA in red and the Rolling sum in blue, for a set of spectral windows for high energy sources. The absolute metric is shown (not scaled by the detection threshold). Both background methods produce similar results using KUT nuisance rejection. As well, the metric is relatively flat over the large steps in count rate, and less than a typical detection threshold of 7-8 for all background jumps.

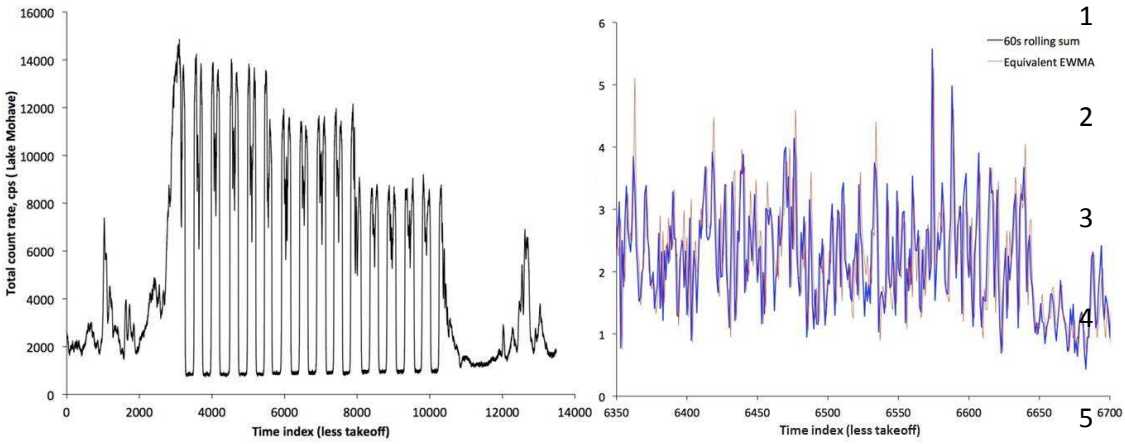

Figure 9. Lake Mohave flight data showing total count rate (left) with NSCRAD Metric results for land-water interface.

4 Conclusion

The spectral anomaly methods described here, with nuisance rejection, have demonstrated the capability for adaptation to aerial detection. The optimization process includes adjustment of energy regions or windows for a particular set of threat and nuisance sources, based on the given detector response function. It was demonstrated that optimization of windows is needed both for differences in application, such as ground-based detection vs. aerial detection, as well as different detector geometries. Results with energy windows optimized for a specific aerial detection system show the ability for improved detection of threat sources and rejection of background-induced false-alarms encountered in aerial detector search applications.

As well, the optimization of KUT nuisance rejection for a given aerial detector system shows promise for improved rejection of the false alarms caused by sharp steps in background. This optimization was demonstrated with real flight data over a land/water interface, which included both sharp count rate steps and spectral changes. The results showed that with adapted KUT nuisance rejection, the steps were largely eliminated and remained below the detection

thresholds. The addition of KUT rejection with optimized energy windows also showed a reduction in the effects of altitude changes during flight, eliminating the need for altitude specific thresholds. Future work will investigate the dependence of energy windows KUT nuisance rejection on specific backgrounds for aerial detection, to determine if sensitivity improves with use of background-specific windows in certain scenarios such as a land/water interface.

5 Acknowledgements

This work has been supported by the US Department of Homeland Security, Domestic Nuclear Detection Office, under competitively awarded contract/IAA HSHQDC-12-X-00376. This support does not constitute an express or implied endorsement on the part of the Government. This report is PNNL-SA-103907. Pacific Northwest National Laboratory is operated for the U.S. Department of Energy by Battelle under Contract DE-AC05-76RL01830.

6 References

[1] D. M. Pfund, R. C. Runkle, K. K. Anderson, and K. D. Jarman, "Examination of Count-Starved Gamma Spectra Using the Method of Spectral Comparsion Ratios," IEEE Trans. Nucl. Sci., vol. 54, no. 4, pp. 1232-1238, Aug. 2007.

[2] R. C. Runkle, M. J. Myjak, S. D. Kiff, D. E. Sidor, S. J. Morris, J. S. Rohrer, K. D. Jarman, D. M. Pfund, L. C. Todd, R. S. Bowler, and C. A. Mullen, "Lynx: An unattended sensor system for detection of gamma-ray and neutron emissions from special nuclear materials," Nucl. Instrum. Methods Phys. Res. A, vol. A598, pp. 815–825, 2009.

[3] R. C. Runkle, M. F. Tardiff, K. K. Anderson, D. K. Carlson, and L. E. Smith, “Analysis of spectroscopic radiation portal monitor data using principal components analysis,” IEEE Trans. Nucl. Sci., vol. 53, no. 3, pp. 1418–1423, Jun. 2006.

[4] R. C. Runkle, T. M. Mercier, K.K. Anderson, and D. K. Carlson, “Point source detection and characterization for vehicle radiation portal monitors,” IEEE Trans. Nucl. Sci., vol. 52, no. 6, pp. 3020–3025, Dec. 2005.

[5] Carolyn E. Seifert, Mitchell J. Myjak, and David M. Pfund Pacific Northwest National Laboratory, “Detection of Anomalous Gamma-Ray Spectra for On-Site Inspection,” The International Scientific Studies Project 2009 Conference Proceedings (ISS 2009).

[6] B. Ng, Survey of Anomaly Detection Methods Lawrence Livermore National Laboratory, Livermore, CA, Tech. Rep. UCRL-TR-225264, Oct. 2006.

[7] K. K. Anderson, K. D. Jarman, M. L. Mann, D. M. Pfund, R. C. Runkle, “Discriminating nuclear threats from benign sources in gamma-ray spectra using a spectral comparison ratio method,” Journal of Radioanalytical and Nuclear Chemistry, vol. 276, no.3 (2008) 713–718.

[8] J. H. Ely, R. T. Kouzes, J. E. Schweppe, E. R. Siciliano, D. M. Strachan, and D. R. Weier, “The use of energy windowing to discriminate SNM from NORM in radiation portal monitors,” Nucl. Instrum. Methods Phys. Res. A, vol. A560, pp. 373–387, May 2006.

[9] David Michael Pfund, Kenneth D. Jarman, Brian D. Milbrath, Member, IEEE, Scott D. Kiff, Member, IEEE, and Daniel E. Sidor, “Low Count Anomaly Detection at Large Standoff Distances,” IEEE Trans. Nucl. Sci., vol. 57, no. 1, Feb. 2010.

[10] Kenneth D. Jarman, Robert C. Runkle, Kevin K. Anderson, David M. Pfund, “A comparison of simple algorithms for gamma-ray spectrometers in radioactive source search applications,” Applied Radiation and Isotope, vol. 66 pp. 362–371, 2008.